



OPEN ACCESS

EDITED BY

Yi Xu,
Horia Hulubei National Institute for
Research and Development in Physics
and Nuclear Engineering (IFIN-HH),
Romania

REVIEWED BY

Giovanni Luca Guardo,
Laboratori Nazionali del Sud (INFN), Italy
Rosario Gianluca Pizzone,
University of Catania, Italy

*CORRESPONDENCE

Giovanni Francesco Ciani,
✉ giovanni.ciani@ba.infn.it
Ragandeep Singh Sidhu,
✉ ragan.sidhu@ed.ac.uk

RECEIVED 20 October 2023

ACCEPTED 05 December 2023

PUBLISHED 04 January 2024
















CITATION

Ananna C, Barbieri L, Boeltzig A,
Campostrini M, Casaburo F, Ciani GF,
Compagnucci A, Gesuè RM, Marsh J,
Masha E, Mercogliano D, Rapagnani D,
Robb D, Sidhu RS and Skowronski J
(2024), Recent results and future
perspectives with solid targets at LUNA.
Front. Astron. Space Sci. 10:1325053.
doi: 10.3389/fspas.2023.1325053

COPYRIGHT

© 2024 Ananna, Barbieri, Boeltzig,
Campostrini, Casaburo, Ciani,
Compagnucci, Gesuè, Marsh, Masha,
Mercogliano, Rapagnani, Robb, Sidhu
and Skowronski. This is an open-access
article distributed under the terms of the
[Creative Commons Attribution License
\(CC BY\)](https://creativecommons.org/licenses/by/4.0/). The use, distribution or
reproduction in other forums is
permitted, provided the original author(s)
and the copyright owner(s) are credited
and that the original publication in this
journal is cited, in accordance with
accepted academic practice. No use,
distribution or reproduction is permitted
which does not comply with these terms.

Recent results and future perspectives with solid targets at LUNA

Chemseddine Ananna ¹, Lucia Barbieri ²,
Axel Boeltzig ³, Matteo Campostrini ⁴,
Fausto Casaburo ⁵, Giovanni Francesco Ciani ^{6*},
Alessandro Compagnucci ⁷, Riccardo Maria Gesuè ⁷,
Jordan Marsh ², Eliana Masha ³, Daniela Mercogliano ¹,
David Rapagnani ¹, Duncan Robb ²,
Ragandeep Singh Sidhu ^{2*} and Jakub Skowronski ⁸

¹Università Degli Studi di Napoli Federico II and INFN Sezione di Napoli, Napoli, Italy, ²Scottish Universities Physics Alliance, School of Physics and Astronomy, University of Edinburgh, Edinburgh, United Kingdom, ³Helmholtz-Zentrum Dresden-Rossendorf, Dresden, Germany, ⁴National Institute of Nuclear Physics, Laboratori Nazionali di Legnaro, Legnaro, Italy, ⁵Università Degli Studi di Genova and INFN Sezione di Genova, Genova, Italy, ⁶Università Degli Studi di Bari and INFN Sezione di Bari, Bari, Italy, ⁷Gran Sasso Science Institute, L'Aquila, Italy, ⁸Università Degli Studi di Padova and INFN Sezione di Padova, Padova, Italy

The stellar evolution and chemical make-up of the Universe are determined by nuclear reactions occurring in a wide variety of stellar sites. Precise determinations of the cross sections of these reactions are crucial for the calculation of reaction rates and for the development of stellar evolution models. The Laboratory for Underground Nuclear Astrophysics (LUNA) collaboration has been at the forefront of the direct measurement of nuclear reactions at the low energies of astrophysical interest for the last 35 years. The many significant results achieved at LUNA have been made possible due to the low background conditions uniquely available thanks to its location deep underground at the Laboratori Nazionali del Gran Sasso. Another key aspect of these successes is due to the experience of the LUNA collaboration in the production and characterization of a variety of solid targets used in reaction measurements. In this review, the main production techniques of solid targets are described, as well as the common methods adopted for target degradation monitoring. We also present the results of recent measurements using these targets and the future plans of the LUNA collaboration for measurements using solid targets at the LUNA400 kV and the new Ion Beam Facility (IBF) 3.5 MV are also presented.

KEYWORDS

solid target, evaporation, sputtering, cross section measurement, nuclear astrophysics

1 Introduction

A comprehensive understanding of the processes that dictate a star's life cycle requires a collaborative effort across various fields, including astronomical observations, theoretical stellar modeling, and experimental nuclear physics. Nuclear astrophysics aims to connect these different fields, to better understand the stellar evolution and the subsequent

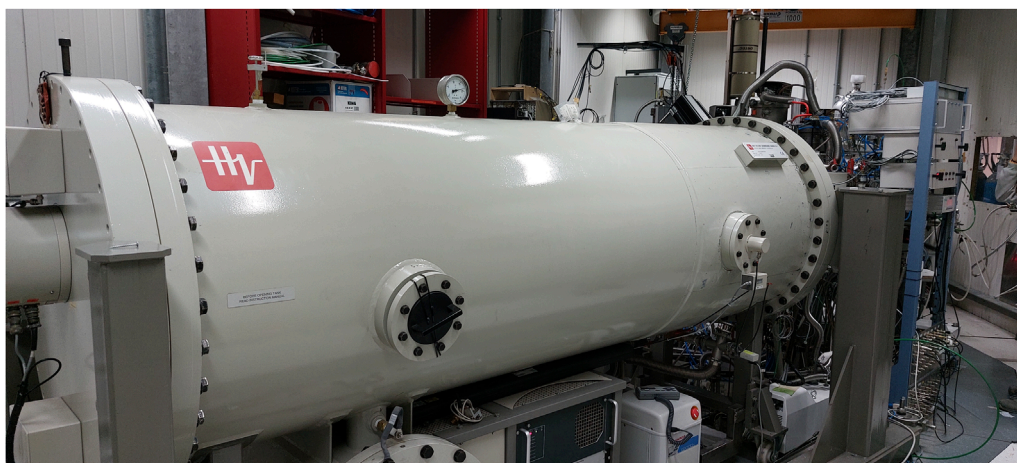


FIGURE 1
The LUNA400 kV accelerator.

impact on the chemical make-up of the Universe. In particular, nuclear physics contributes to the measurement of the cross sections of reactions that occur in stellar environments. In quiescent scenarios, nuclear reactions serve a dual function. Firstly, reactions produce the energy required to fight against the gravitational collapse of the star, a battle that rages throughout the star's long life. Furthermore, nuclear reactions are the mechanism by which all elements in the periodic table are synthesized. Direct measurements of the nuclear reaction cross sections are therefore crucial to better model these stellar environments so that we can better understand the stellar and chemical evolution of the Universe. At the energies of interest for astrophysics, the cross sections of the reactions involved are often at the level of nanobarn or lower and therefore difficult to measure. Measurements at surface laboratories can be extremely challenging, mainly due to the high environmental (radioactivity and muonic components) background present above ground. In order to reduce this background, the LUNA experiment was installed underground at INFN Laboratori Nazionali del Gran Sasso (LNGS) (Italy). The natural shielding of 1,400 m of rocks (3,800 m of water equivalent), reduces the muon and neutron components of the cosmic background by a factor of 10^6 and 10^3 respectively, with respect to Earth's surface, allowing measurements not feasible in surface laboratories because of low signal to noise ratio [Cavanna and Prati \(2018\)](#). Many of these reactions have involved solid targets whose composition and thickness must be well known and must withstand the intense beams of the LUNA accelerators. The success of many experimental campaigns has been dependent on the development of techniques for the production and monitoring of these targets, which has been achieved for a wide range of nuclei of interest for reaction studies.

Different accelerators have been used at LUNA in the last 35 years. A 50 kV machine [Greife et al. \(1994\)](#), now decommissioned, was mainly used to study hydrogen burning reactions relevant to the Sun, and produced pioneering results (e.g., [Junker et al., 1998](#)). In 2001, a 400 kV machine was installed and is still in operation today, with a focus on the reactions part of the Carbon-Nitrogen-Oxygen (CNO) and NeNa cycles in Asymptotic

Giant Branch (AGB) stars ([Ananna et al., 2021](#); [Masha et al., 2023](#)). The LUNA400 kV accelerator ([Figure 1](#)) is a commercial single-ended electrostatic accelerator, that can provide stable and intense ($I = 200 \mu\text{A}$) proton or alpha beams with high energy resolution (30 eV) [Formicola et al. \(2003\)](#). The beam from the LUNA400 kV machine can be focused either onto a windowless extended gas target or a solid target, allowing for a range of measurements to be performed. Very recently, the LUNA collaboration entered into a new phase with the installation of a 3.5 MV accelerator. This machine is an Inline Cockcroft Walton accelerator, able to provide ion beams of H^+ , $^4\text{He}^+$ and $^{12}\text{C}^+$ and $^{12}\text{C}^{++}$ in the energy range from 0.35 MeV to 3.5 MeV [Sen et al. \(2019\)](#). With this machine, the LUNA collaboration will study nuclear reactions important for advanced phases of stellar evolution, such as helium and carbon burning ([Ferraro et al., 2021](#)).

In this review, several techniques to produce and characterize solid targets will be presented, together with the most recent measurements performed at LUNA irradiating solid targets. Furthermore, the future developments required for the next phase of solid target measurements at LUNA using the LUNA400 kV and new 3.5 MV Bellotti facility will be presented.

2 Solid targets in nuclear astrophysics

At the LUNA400 kV, both gaseous and solid targets can be irradiated for nuclear astrophysics measurements. Solid targets have the advantage of a higher average density compared to gaseous targets, typically by an order of magnitude, in addition to the practical advantage of more compact experimental setups than typical gaseous extended targets. The solid targets used at LUNA have been produced using several different techniques, e.g. evaporation, reactive sputtering, oxidation, and implantation [Imbriani et al. \(2005\)](#). The production technique depends on the target nucleus under study and its chemical behavior. In all production methods, the target material is generally deposited on a metallic disk made with a high atomic number material, e.g.,

tantalum, gold, or copper. At LUNA, 0.25 mm thick tantalum disks with a 4 cm diameter have often been used because they are less expensive and easier to machine with respect to other options. The Coulomb barrier for these elements is so high that it is very unlikely to generate reactions with the beam projectiles, ideal for suppression of background from the backing material. Nevertheless, light element impurities (e.g., deuterium, oxygen, fluorine) can be present in the backing, generating some beam induced background events. In order to minimize the surface contamination, backings are rinsed with isopropyl alcohol and with a 2% solution of detergent in an ultrasonic bath and then they are left for several hours in a solution with citric acid at 5% to 10% with 1% H₂O₂ added. To prevent carbon deposition on target during beam irradiation, a phenomenon called carbon build-up, the beam passes through a cold trap made of a 1 m long copper tube cooled with liquid nitrogen, which extends along the beam line and up close to the target [Di Leva et al. \(2014\)](#). This allows contaminants to freeze out on the copper, suppressing the build-up of impurities on the target during irradiation.

The average density of solid targets generally varies between 5×10^{17} atoms/cm² and 2×10^{18} atoms/cm². It is crucial that target characteristics, such as the target thickness and target composition, are evaluated with high precision in order to reduce systematic uncertainties in the final cross section determination. The reaction cross section $\sigma(E)$ can be extracted from a measurement using the Eq. 1:

$$Y = \int_{E_b - \Delta E}^{E_b} \frac{\sigma(E)}{\epsilon_{\text{eff}}(E)} dE, \quad (1)$$

where Y is the experimental yield, namely the number of emitted particles per projectile, E_b the beam energy, $\epsilon_{\text{eff}}(E)$ the effective stopping power, and ΔE the projectile energy loss in the target. The effective stopping power depends on the target composition, as explained in Bragg's addition rule parametrized as in Eq. 2:

$$\epsilon_{\text{eff}}(E) = \epsilon_a + \sum_a \frac{N_i}{N_a} \epsilon_i, \quad (2)$$

where $\frac{N_i}{N_a}$ is the ratio between inactive and active nuclei, and ϵ_a and ϵ_i are the stopping powers of the corresponding (active and inactive) pure materials.

One drawback of the use of solid targets is their possible deterioration due to the high beam powers, of about 100 W incident on the target, and can occur rapidly over a short timescale. This effect can result in a change in target characteristics such as the density profile, thickness, or stoichiometry that can affect the determination of the cross section if not correctly accounted for. In order to reduce the heating of targets from beam irradiation, backings are water cooled by de-ionized water chilled to temperatures of approximately 5°C. Moreover, a wobbling system installed along the beam line induces an oscillatory motion of the beam spot, increasing the irradiation surface and reducing the power density applied to a single area of the target surface.

Beyond these implementations, the target is monitored throughout the experimental measurement with several experimental techniques, to gauge the condition of the target. A typical online analysis usually employed at LUNA is the so-called resonance scan technique, or Nuclear Resonant Reaction Analysis

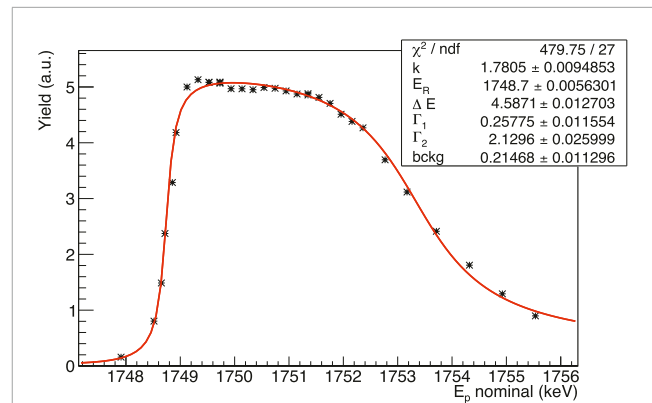


FIGURE 2

Example of excitation function after the $E_R = 1,748$ keV resonance scan of the $^{13}\text{C}(p, \gamma)^{14}\text{N}$ reaction. The fit is represented by the red curve and the parameters as indicated in Eq. 3 are shown in the figure.

(NRRA), which is described in detail in [Rolf and Rodney \(1988\)](#). It consists in exploiting a well known narrow resonance of the reaction under study. The variation of the beam energy in an interval around the energy of the resonance populates the energy deeper and deeper in the target. The excitation function obtained can be parametrized in terms of the resonance strength $\omega\gamma$, target thickness ΔE , and initial beam energy E_p , with a double arctangent shape as in Eq. 3:

$$Y(E_p) = \frac{\lambda^2}{2\pi} \omega\gamma \frac{M+m}{M} \frac{1}{\epsilon} \left[\arctan\left(\frac{E_p - E_R}{\Gamma_1/2}\right) - \arctan\left(\frac{E_p - E_R - \Delta E}{\Gamma_2/2}\right) \right], \quad (3)$$

where the footer R is the quantity that has been calculated at the resonance energy, and the mass ratio (M is the mass of the target nuclei, m is the mass of the projectile) takes into account that the stopping power ϵ is usually given in the laboratory system. One example of fit of the excitation function after the resonance scan of the $^{13}\text{C}(p, \gamma)^{14}\text{N}$ is shown in [Figure 2](#).

There are some cases where no resonance can be populated in the dynamic range of the accelerator. In that case, an innovative and equivalent approach, called γ -shape analysis, can be used. This technique is described in [Ciani et al. \(2020\)](#). Briefly, it is based on the fact that if no resonances are populated, the main contribution to the reaction comes from the direct capture process $A(x, \gamma)B$. Due to beam energy losses with increasing depth within the target, from E_p to $E_p - \Delta E$, in this energy range both the cross section and stopping power can vary as a function of the projectile energy. The γ -rays emitted depend on the beam energy by the relation in Eq. 4 (here Doppler and recoil effects are assumed negligible):

$$E_\gamma = E_{c.m.} + Q \quad (4)$$

In an infinitesimal layer of thickness dE , the infinitesimal yield dY can be evaluated as in Eq. 5:

$$dY(E, E + dE) = \frac{\sigma(E)}{\epsilon(E)} dE \quad (5)$$

Therefore the shape of a primary γ -ray transition acquired with a high energy resolution detector is governed by the behavior

of the reaction cross section $\sigma(E)$ over the energy range covered by the incident beam as it loses energy traversing the target. Also in this case the fit of the primary transition provides information on the target thickness and stoichiometry. Further analysis can be performed offline to confirm and crosscheck the online results in terms of stoichiometry by Ion Beam Analysis techniques, such as Elastic Recoil Detection Analysis (ERDA) or Rutherford Backscattering Spectrometry (RBS) [Nastasi et al. \(2014\)](#).

3 Evaporation of carbon targets

Carbon targets have been recently used at LUNA for the $^{13}\text{C}(\alpha, n)^{16}\text{O}$ [Ciani et al. \(2021\)](#) and $^{12/13}\text{C}(p, \gamma)^{13/14}\text{N}$ [Skowronski et al. \(2023a\)](#) measurements. These were produced by evaporating graphite onto 4 cm diameter tantalum backings. Depending on the target nuclei of the reaction to be measured, the graphite was either natural, with a nominal ^{12}C concentration of 98.9%, or enriched in ^{13}C to a concentration of 99%.

Due to the high melting point of graphite (3,600°C) the evaporation process was conducted using the electron gun technique, employing the Leybold UNIVEX 350 vacuum evaporator at ATOMKI, the Institute for Nuclear Research located in Debrecen, Hungary. The vacuum chamber is shown in [Figure 3](#). The vacuum enclosure of the evaporator comprises a copper liquefaction container, a modifiable arm employed to grasp the tantalum disk positioned at a distance of 10 cm from the liquefaction container, and an electron gun, which produces electrons via thermo-electric effect. The electron beam was properly focused on a carbon pellet inserted in the copper container. The latter was then heated allowing direct evaporation of carbon onto the Ta backing. A quartz oscillator fixed within the vacuum enclosure, at a distance of 15 cm from the liquefaction container, was employed to oversee the evaporation process and give a first rough estimate of the target thicknesses. The key concept behind this is that the ^{13}C powder evaporates isotropically and is deposited also on the quartz. The oscillation frequency will drop as the crystal's mass is increased by the material being deposited on it. An electronic instrument continuously reads the frequency and performs appropriate mathematical functions to convert that frequency data to thickness data, both instantaneous rate and thickness [Ohring \(1992\)](#).

The target thickness obtained through this methodology ranged between 500 and 800 Å.

Targets were characterized immediately after production using the NRA technique at the 2.0 MV Medium-Current Plus Tandem Accelerator installed at ATOMKI ([Csedreki et al., 2020](#)), by exploiting the $E_p = (1747.6 \pm 9)$ keV narrow ($\Gamma = (135 \pm 8)$ eV) resonance of the $^{13}\text{C}(p, \gamma)^{14}\text{N}$ reaction ($Q = 7,550.6$ keV) [Zeps et al. \(1995\)](#). Target characterization was performed before and after irradiation by the LUNA proton beam. After irradiation, it was possible to characterize both the beam spot and off-spot areas of the target, to assess the target degradation experienced during the measurement. The main limitation of this technique is target characterization could only be performed at the beginning and at the end of the experiment since the resonance of interest is out of the dynamic energy range of the LUNA400 kV accelerator.



FIGURE 3

The vacuum chamber of the evaporator. All the main components are indicated by coloured squares: in white the hole where the electron beam comes from, in red the melting pot of the material, in green the nipper where the backing is held, in light blue the quartz used to monitor the evaporation process. The reader can find further information on the working principle of the quartz in the text.

In order to monitor the target condition during the experiment, the γ -shape analysis, described in [section 2](#) was therefore used.

All of the evaporated carbon targets showed great stability under proton irradiation. Target degradation only started to become significant at approximately 10 C of accumulated proton charge, with targets able to withstand irradiation up to a total of 80 C accumulated proton charge. In contrast, target degradation was significantly faster under alpha irradiation. The γ -shape analysis showed a 30% reduction in the yield following approximately 3 C of accumulated charge.

3.1 $^{12/13}\text{C}(p, \gamma)^{13/14}\text{N}$

The $^{12}\text{C}(p, \gamma)^{13}\text{N}$ ($Q = 1,943.5$ keV) and the $^{13}\text{C}(p, \gamma)^{14}\text{N}$ ($Q = 7,550.6$ keV) reactions are important to study the mixing phenomena inside both Red Giant Branch (RGB) and AGB stars. The nuclei produced in the hydrogen burning regions of these stars are usually transported to the stellar surface through convective motions. The mixing is particularly important for AGB stars which undergo several dredge-up cycles [Herwig \(2005\)](#), during which most of the hydrogen burning products enter inside the convective region of the star and are then pushed towards the stellar surface. Nevertheless, contributions other than the convective ones are needed to explain the observed elemental abundance inside the stellar atmosphere [Busso et al. \(2007\)](#). Many different hypotheses have been proposed [Aerts et al. \(2014\)](#), but none of them are able to completely explain the observed surface abundances.

The $^{12/13}\text{C}(p, \gamma)^{13/14}\text{N}$ reactions are a useful tool to constrain these hypotheses. Since the stellar surface $^{12}\text{C}/^{13}\text{C}$ ratio is a well-known observable, knowledge of the precise equilibrium ratio inside the hydrogen burning region at different temperatures can

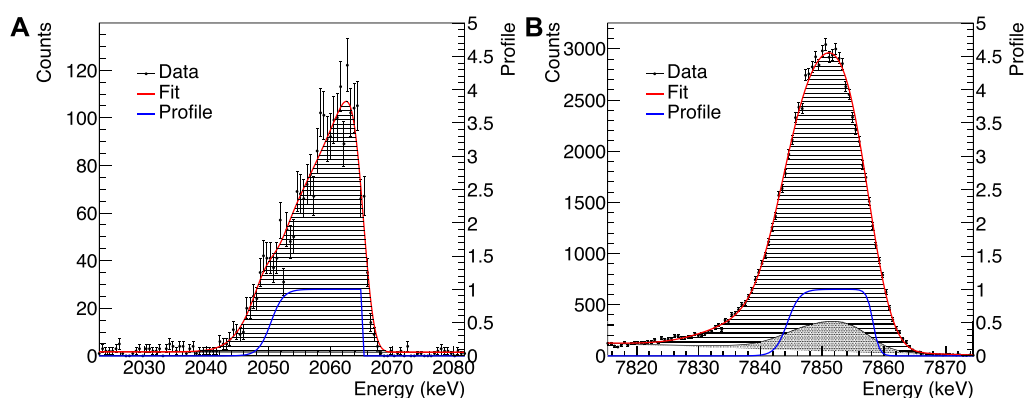


FIGURE 4

The γ -shape analysis fits for the $^{12}\text{C}(p,\gamma)^{13}\text{N}$ reaction (A) and the $^{13}\text{C}(p,\gamma)^{14}\text{N}$ reaction (B) at 130 keV and 330 keV, respectively. The lined regions show the direct capture contribution, whereas the dotted one shows the amount of resonant contribution to the cross section.

help improve stellar models. However, the literature uncertainty of the $^{12/13}\text{C}(p,\gamma)^{13/14}\text{N}$ reaction rates remains very high [$\sim 20\%$ Angulo et al. (1999), Xu et al. (2013)]. In order to reduce the uncertainty at the temperatures of interest for the RGB and AGB stars, both of these two reactions have been recently measured at LUNA.

In order to control and characterize the various systematic uncertainties, two different, but complementary setups were adopted for the measurements. One setup was based on a HPGe detector in close geometry, whereas the other setup utilized a high efficiency Bismuth Germanium Oxide (BGO) scintillator detector Skowronski et al. (2023b). The high energy resolution of the HPGe allowed all the many transitions of the reaction to be studied and also enabled the use of the γ -shape technique to characterize the target throughout the measurement. The technique was used to extract both the information regarding the target thickness and also to derive the cross section of the reactions. The target information was first tuned with the NRRA measurements, then the fit was performed leaving the cross section as a free parameter. Two examples of the fit are shown in Figure 4. The setup utilizing the BGO scintillator facilitated measurements at lower proton energies due to the high efficiency of the BGO detector. In the case of the $^{13}\text{C}(p,\gamma)^{14}\text{N}$ reaction, total absorption spectroscopy was applied. The cross section could easily be extracted as the reaction Q -value of 7,551 MeV, meaning that the sum-peak of interest lay in a region of the sum spectrum free from any background contributions. In contrast, the $^{12}\text{C}(p,\gamma)^{13}\text{N}$ reaction has a Q -value of 1,943 MeV, and the sum-peak lay in a region affected by the internal background of the BGO, and the cross section could not be easily extracted. Consequently, the cross section was studied using the activation technique, since ^{13}N is β^+ unstable Skowronski et al. (2023b). This technique resulted in a drastic reduction in the background by exploiting the 511 keV coincidences.

All the measurements were successfully performed and precise cross section values in both the RGB and AGB regions of interest were published in Skowronski et al. (2023a). The astrophysical impact on the mixing phenomena is currently under study and will be published in a devoted paper.

3.2 $^{13}\text{C}(\alpha,n)^{16}\text{O}$

$^{13}\text{C}(\alpha,n)^{16}\text{O}$ is the main source of neutrons required for the synthesis of $90 \leq A \leq 204$ elements in the Universe through the slow neutron capture process. The low neutron flux produced by $^{13}\text{C}(\alpha,n)^{16}\text{O}$, results in the average time for an unstable isotope to decay being significantly smaller than the average time required for further neutron captures, such that neutron capture occurs only on isotopes in the valley of stability Bisterzo et al. (2015). Low mass ($< 3 M_{\odot}$) Asymptotic Giant Branch stars are the most relevant stellar sites where $^{13}\text{C}(\alpha,n)^{16}\text{O}$ is the source of s -process neutrons. A ^{13}C pocket forms between the intermediate He layer (where the 3α process forms ^{12}C) and the external H layer (where after $^{12}\text{C}(p,\gamma)^{13}\text{N}$, ^{13}C is formed by β^- decay of ^{13}N). During so-called thermal pulsing periods Straniero et al. (2006); Gallino et al. (1998), the ^{13}C pocket reacts with the surrounding alpha particles at typical temperatures of 90 MK producing a slow neutron flux of $N_n \approx 1 \times 10^7$ neutrons/cm³ in long periods of 10^4 years Käppeler et al. (2011).

To properly account for the s -process neutron budget, an accurate determination of the $^{13}\text{C}(\alpha,n)^{16}\text{O}$ stellar reaction rate is required. Several direct measurements have previously been performed Sekharan et al. (1967), Davids (1968), Bair and Haas (1973), Kellogg et al. (1989), Drotleff et al. (1993), Harissopoulos et al. (2005), Heil et al. (2008). These measurements were all performed in surface laboratories so that natural background limited the investigations to energies approaching the Gamow window, E_G ($150 \text{ keV} < E_G < 230 \text{ keV}$) and affected the final precision achievable.

In parallel, also different indirect techniques have been used. For example, in Trippella and Cognata (2017), the asymptotic normalization coefficient (ANC) and the Trojan Horse Method have been combined for an independent evaluation of the astrophysical factor.

Recently, both LUNA Ciani et al. (2021) and Jinping Underground experiment for Nuclear Astrophysics (JUNA) Gao et al. (2022) pushed measurements of the $^{13}\text{C}(\alpha,n)^{16}\text{O}$ reaction to lower energies, approaching the Gamow window, thanks to the

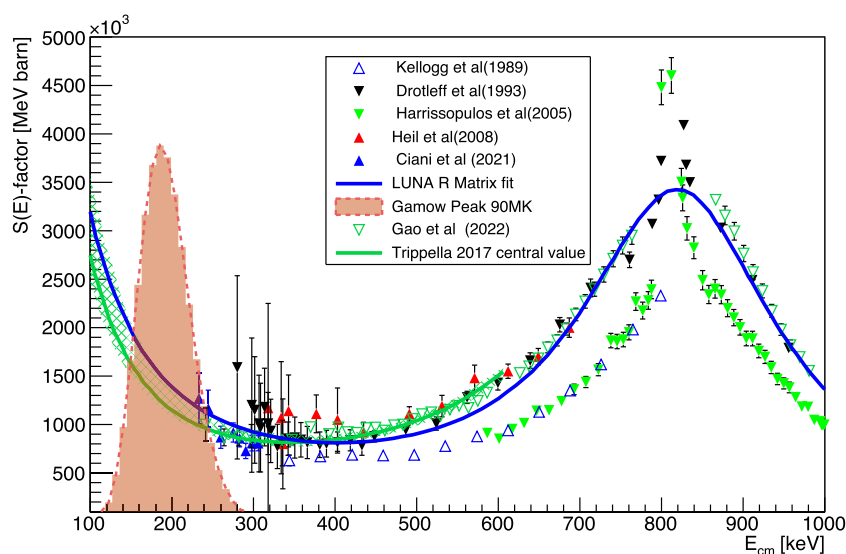


FIGURE 5

S(E)-factor of the $^{13}\text{C}(\alpha, n)^{16}\text{O}$ reaction. Different data sets are indicated by different styles and colors as indicated in the legend. All the data in the plot are direct data, except from [Trippella and Cognata \(2017\)](#) that used the indirect technique of the Trojan Horse Method. Figure is adapted from [Ciani et al. \(2021\)](#) and more recent data from [Gao et al. \(2022\)](#) have been added.

low background environment of deep underground laboratories. As a consequence, both the accuracy and the precision of extrapolations to lower energies, required by stellar models, were increased.

In particular, the LUNA measurement of $^{13}\text{C}(\alpha, n)^{16}\text{O}$ was performed using the LUNA400 kV accelerator with a high intensity ($I \sim 150 \mu\text{A}$) He^+ beam impinging on evaporated ^{13}C targets. The neutron detection array, described in detail by [Csedreki et al. \(2021\)](#), consisted of 18 ^3He proportional counters installed in two concentric rings around the reaction chamber in a polyethylene moderator. To reduce the intrinsic background of the detectors, which in deep underground laboratories can be a major contributor to the detection sensitivity [see, e.g., [Alimonti et al. \(1998\)](#)], detectors with stainless steel walls were employed instead of the standard aluminum walls. Moreover, the use of pulse shape discrimination allowed for a further reduction of the background to $1.3 \pm 0.2 \text{ counts/h}$ through the identification of detected particles [Balibrea-Correa et al. \(2018\)](#). This background is about two orders of magnitude lower with respect to experiments in surface laboratories.

Two detector array configurations were employed; a vertical array with a multi-target chamber for a faster target characterization in the first campaign, and a horizontal array with a single target chamber, to maximize detection efficiency. The array configurations were evaluated using GEANT4 simulations and validated with experimental measurements using the activation technique with the $^{51}\text{V}(p, n)^{51}\text{Cr}$ reaction and with a calibrated AmBe source. The detection efficiency achieved at the relevant neutron energies, between 2 and 2.5 MeV, was $(38 \pm 3)\%$ and $(34 \pm 3)\%$ for the horizontal and vertical configurations respectively [Csedreki et al. \(2021\)](#). During the measurement campaign, 100 targets were irradiated for a total accumulated charge of 300 C.

Data taking at LUNA consisted of long α -beam runs with accumulated charges of ≈ 1 C per run, interspersed by short proton-beam runs with the moderator opened and HPGe detector in

close geometry, with typical accumulated charges of 0.2 C. The target degradation was checked using gamma shape analysis during the proton runs, by the $^{13}\text{C}(p, \gamma)^{14}\text{N}$ reaction with the HPGe detector. Thanks to the impressive background suppression by the Gran Sasso massif (the muon component of the cosmic ray is reduced by a factor of 10^6 and the neutron component by a factor of 10^3) and by using a novel approach to target degradation monitoring, the LUNA collaboration measured the $^{13}\text{C}(\alpha, n)^{16}\text{O}$ reaction cross section in the energy range $230 < E_{\text{c.m.}} < 305$ keV, approaching the high energy edge of the Gamow window. Notably, the achieved uncertainty was 20% lower than in previous measurements [Ciani et al. \(2021\)](#). Measured cross sections were included in an Monte Carlo (MC) *R*-matrix analysis, together with most recent direct measurements results ([Drotleff et al., 1993](#); [Harissopoulos et al., 2005](#); [Heil et al., 2008](#)). Further details can be found in [Ciani et al. \(2021\)](#). The results of the LUNA measurements are summarized in [Figure 5](#) together with the most recent literature data and the *R*-matrix fit.

It is worth noting that the *R*-matrix calculation is strongly dominated by the large uncertainties of other datasets (e.g., [Drotleff et al., 1993](#); [Heil et al., 2008](#)) Therefore in the near future LUNA collaboration is planning to extend the measurement in the energy range $400 < E_{\alpha} < 900$ keV to provide a unique dataset with reduced and well controlled systematic uncertainties.

The astrophysical reaction rate per particle pair $\langle \sigma v \rangle$ as a function of stellar temperature was calculated by integrating the *R*-matrix cross section. Thanks to the excellent quality of the data, the reaction rate at $T = 0.1$ GK was evaluated with an overall uncertainty of approximately 15%. In particular, the reaction rate was considered at $\sim 95\%$ uncertainty, where more ^{13}C survives and is subsequently burned at a higher temperature (~ 200 MK) in a convective shell powered by the following thermal pulse. This generates a second neutron burst characterized by higher neutron density and lower

exposure. For stars of nearly solar composition (metallicity $Z = 0.02$, and $Y = 0.27$), this causes considerable variations of some isotopic abundances. In particular, isotopes close-by branching points that are sensitive to the neutron density are strongly influenced. In particular ^{205}Pb , and ^{152}Gd are reduced by 15% and ^{60}Fe might increase by 105% as described in [Ciani et al. \(2021\)](#).

4 Evaporation of sodium and lithium targets

Sodium and lithium targets, produced by evaporation, have also been used by the LUNA collaboration in several measurements. The melting points of sodium and lithium are significantly lower than that of carbon (97°C and 180°C, respectively), and therefore they do not require heating using the electron gun process discussed in the previous section. Instead, the sample material is heated under vacuum in a crucible. The evaporated material is then deposited onto the backing which is mounted on top of the crucible. In general, heating is slower and more controlled using this process compared to heating using the electron gun. In this section, the use of both sodium and lithium targets at LUNA are further discussed, including the measurements in which they have been utilized.

4.1 Lithium targets

The discrepancy in the lithium abundance between astronomical observations and theoretical calculations is a long-standing open question in nuclear astrophysics. This discrepancy is not isolated to one astrophysical scenario but instead is a broad problem in nuclear astrophysics which is impacted by various nucleosynthesis mechanisms. One aspect of this broad discrepancy between theory and observations is known as the cosmological lithium problem, which refers to the observation that the ^7Li abundance of metal-poor stars in the galactic halo is approximately 3 times lower than the predicted Big Bang Nucleosynthesis (BBN) abundance as described in [Tanabashi et al. \(2018\)](#). Another point of tension between theory and observation is in the $^6\text{Li}/^7\text{Li}$ isotopic ratio. The observed Solar System isotopic ratio of 0.08 [Lodders \(2003\)](#) is significantly larger than the predicted BBN ratio which is of the order of 10^{-5} , with it suggested that less than half of the lithium in the Solar system was produced by BBN but instead is produced from stellar sources such as red giants, low mass asymptotic giant branch stars, or novae. In this context, it has been suggested to use the $^6\text{Li}/^7\text{Li}$ isotopic ratio as a tool to constrain non-standard lithium production mechanisms ([Prantzos, N. 2012](#)). One crucial reaction which directly impacts the ratio between the two lithium isotopes is the $^6\text{Li}(p,\gamma)^7\text{Be}$ ($Q = 5,606$ keV) reaction that converts ^6Li to ^7Li , following the decay from ^7Be . However, the cross section of this reaction was uncertain, with a new, previously unobserved resonance at $E_{c.m.} = 195$ keV suggested in a paper by [He et al. \(2013\)](#). To investigate the existence of this resonance, the $^6\text{Li}(p,\gamma)^7\text{Be}$ reaction was the subject of an experimental campaign at LUNA, using solid lithium targets, which is described in detail by [Piatti et al. \(2020\)](#). The targets were produced by evaporating 95% enriched lithium compounds, such as lithium oxide ($^6\text{Li}_2\text{O}$) or lithium tungstate $^6\text{Li}_2\text{WO}_4$ onto tantalum backings. The average nominal target thickness was $50 \mu\text{g cm}^{-2}$.

Target stability was monitored by comparing the experimental yield during periodic irradiation (after the accumulation of 10 C) at a fixed beam energy, $E_p = 290$ keV. The yield in the observed Region Of Interest (ROI) remained constant for $^6\text{Li}_2\text{O}$, opposed to the $^6\text{Li}_2\text{WO}_4$ targets, where a decrease of approximately 20% was observed. Following the measurement at LUNA, the target thickness and profile were independently evaluated using the NRR and ERDA techniques at the HZDR laboratory (Dresda, Germany).

The γ -rays emitted from the $^6\text{Li}(p,\gamma)^7\text{Be}$ reaction were detected using a HPGe detector in close geometry, in addition to alpha and ^3He particles from the $^6\text{Li}(p,\alpha)^3\text{He}$ reaction. The cross section of the $^6\text{Li}(p,\alpha)^3\text{He}$ reaction was known to 5% precision prior to the experiment, allowing verification of the $^6\text{Li}(p,\gamma)^7\text{Be}$ cross section relative to the $^6\text{Li}(p,\alpha)^3\text{He}$ cross section. The $^6\text{Li}(p,\gamma)^7\text{Be}$ cross section was determined in the energy range from 60 to 350 keV with statistical and systematic uncertainties of 2% and 13% respectively. This precision was sufficient to conclusively exclude the existence of the resonance at 195 keV. In addition to this, the stellar reaction rate was reduced with respect to previous compilations [33% lower than [Xu et al. \(2013\)](#)], and the accuracy was improved by 10%. The LUNA results have recently been confirmed by an indirect determination of the $S(E)$ factor with the asymptotic normalization coefficient method [Kiss et al. \(2021\)](#) and by calculation of [Dubovichenko et al. \(2022\)](#). The astrophysical factor $S(E)$ as a function of the center of mass energy for the different targets used in the experiment is shown in [Figure 6](#).

4.2 Sodium targets

Sodium is primarily involved in the neon-sodium (NeNa) cycle of hydrogen burning. This cycle can take place in many important astrophysical environments with $T \geq 0.05$ GK, such as in the H-shell of red giants and AGB stars, novae, and in the cores of massive stars. Nucleosynthesis involving sodium is also significant for the production of higher mass isotopes. Proton capture on ^{23}Na determines either the closure of the NeNa cycle through the (p,α) reaction or a leak of cycle material towards the Mg-Al cycle via the (p,γ) radiative capture [Hale et al. \(2004\)](#). The rate of these two reactions affects the final yields of the involved nuclides and the extent of sodium destruction in the stellar environment. More accurate knowledge of this latter process could prove crucial in a greater understanding of Globular Clusters (GC). GC are tight spherical distributions of old gravitationally bound stars, orbiting in the extended halos of most spiral galaxies. They constitute a rather unique probe of galactic and stellar evolution theory [Gratton et al. \(2012\)](#), but their formation and peculiar chemical evolution are still not completely understood [Gratton et al. \(2019\)](#). Their most striking feature is the presence of multiple stellar populations [Carretta, E. et al. \(2010\)](#); [Piotto et al. \(2007\)](#) showing strong star-to-star variations in light elements abundances. In particular, secondary generation stars appear to be depleted in C and O, enriched in He, N, and Na, but have a rather constant $[\text{Fe}/\text{H}]$, proving that a contribution to their formation from supernovae-processed material is in most cases unlikely ([Renzini et al., 2015](#)).

To explain such chemical signatures, several scenarios have been proposed as the origin of second generation stars' composition. These range from fast rotating massive stars [Krause et al. \(2013\)](#),

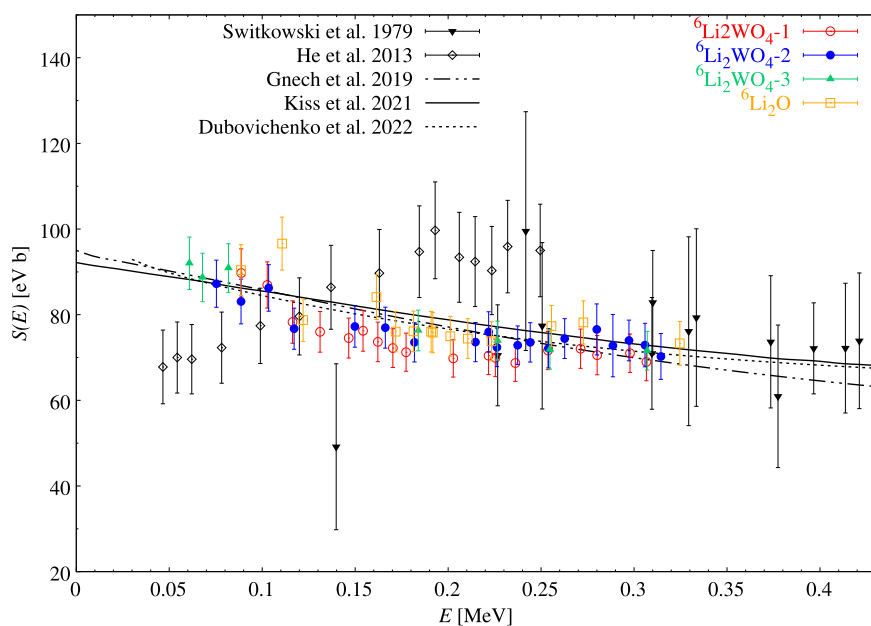


FIGURE 6

Astrophysical $S(E)$ - factor extracted for different targets used in the LUNA campaign. LUNA results are in agreement using different targets with different stoichiometry and with theoretical calculation by [Gnech and Marcucci \(2019\)](#), showing a monotonic energy dependence, excluding the presence of the resonance at $E_p = 195$ keV.

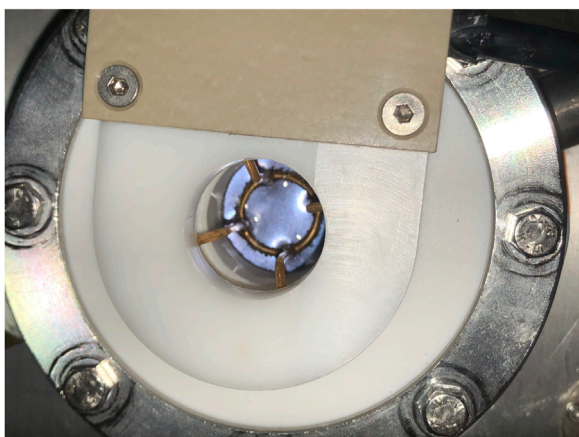


FIGURE 7

Detail of the anodization setup, view from top. The Ta backing is mounted in the Teflon holder and the golden anode basket is moved in the vicinity of the backing.

to a single supermassive star [Denissenkov and Weiss \(2004\)](#) and AGB stars [D'Ercole et al. \(2008\)](#), [D'Antona et al. \(2016\)](#). However, recent observational constraints have excluded the majority of these scenarios [Renzini et al. \(2015\)](#), leaving AGB stars as the most suitable candidate polluters, in a scenario also known as self-enrichment. In AGB stars with $M \geq 4M_{\odot}$ the NeNa cycle may be onset together with the hot-CNO cycle at the basis of the convective envelope, in a process known as Hot Bottom Burning (HBB). When the convective envelope reaches down to the H-burning shell, all

the processed material can be dredged up to the stellar surface. This material is ejected into the interstellar medium, from which the next-generation of stars is later born. The main problem with this scenario is the observed O-Na anti-correlation. Observations of GC stars have revealed that they are O-poor and Na-rich, which cannot be reproduced by AGB stellar models. One possible solution to this long-standing problem, suggested by many authors ([Ventura and D'Antona, 2006](#); [Renzini et al., 2015](#)), would be a decrease in the $^{23}\text{Na}(p, \alpha)^{20}\text{Ne}$ reaction rate by a factor ≈ 4 to 5 than currently adopted from [Angulo et al. \(1999\)](#). This would increase the temperature range where Na is destroyed faster than O, producing the observed anti-correlation in AGB models without affecting other successes of these models such as the proton capture production of Al, Si, and K ([Ventura et al., 2012](#)). LUNA experimental campaigns dedicated to the study of the competing $^{23}\text{Na}(p, \gamma)^{24}\text{Mg}$ ($Q = 11,692.69 \pm 0.01$ keV) and $^{23}\text{Na}(p, \alpha)^{20}\text{Ne}$ ($Q = 2,376.133 \pm 0.002$ keV) reactions was conducted to explore this theory further. These measurements are presented in the following sections.

4.2.1 $^{23}\text{Na}(p, \gamma)^{24}\text{Mg}$

^{23}Na is the only stable isotope of sodium, so no enrichment is required during target production. In previous studies, targets have been produced by either implantation or by evaporation. Sodium targets produced by implantation have been reported by several authors ([Seuthe et al., 1987](#); [Brown et al., 2009](#); [Cesaratto, 2011](#)). The targets were produced by raster scanning a ^{23}Na ion beam over the surface of a backing disk, typically at energies between 10 and 30 keV. Several materials have been used as backings, but the best results in terms of homogeneity profile, high sodium concentration, and stability are nickel [Seuthe et al. \(1987\)](#) and copper [Brown et al. \(2009\)](#). A more recent attempt to produce targets

by implantation by Cesaratto (2011) failed to produce targets with sufficient sodium concentrations or homogeneous target profiles using several different backing materials.

Evaporated targets have shown better performance in terms of target stability and reproducibility in target production. These targets were produced at ATOMKI evaporating sodium compounds onto Ta backings. The choice of the sodium compound used to produce the target requires consideration of several factors, including stoichiometry, ease of production, and target stability. The majority of sodium salts are also hygroscopic, i. e., the stoichiometry of the target changes when exposed to humidity. This requires careful heating procedures and can affect the reproducibility of targets when certain compounds are used. In the $^{23}\text{Na}(p,\gamma)^{24}\text{Mg}$ measurement at LUNA, targets were produced using three different target materials, NaCl , Na_2WO_4 and Na_2SiO_3 . The best target properties were obtained using Na_2WO_4 . Characterization of targets was conducted by NRRRA using the strong resonance at $E_p = 309$ keV ($\omega\gamma = (105 \pm 19)$ meV) in the $^{23}\text{Na}(p,\gamma)^{24}\text{Mg}$ reaction. The typical target thickness was $50 \mu\text{g cm}^{-2}$, and the typical accumulated charge on each target was 10 C–30 C.

The $^{23}\text{Na}(p,\gamma)^{24}\text{Mg}$ reaction can populate many excited states of the compound nucleus, but only a few are relevant for the determination of the astrophysical reaction rate (Wang et al., 2012). In stellar environments with temperatures up to 1 GK, the reaction rate is predominantly influenced by the non-resonant cross section and two narrow resonances located at lower energies ($E_p = 140$ keV and 251 keV). These resonances play a significant role in shaping the overall reaction rate and subsequent nucleosynthesis processes in stellar scenarios. The strengths of both of these resonances were measured at LUNA using a proton beam impinging on Na_2WO_4 targets Boeltzig et al. (2019). Two complementary detection approaches were employed for the measurement. For the weaker 144 keV resonance, a 4π BGO detector with high efficiency was used. For the stronger 251 keV resonance, a high-resolution HPGe detector was employed. The resonance strength determined for the 140 keV resonance was $\omega\gamma = 1.46^{+0.58}_{-0.53}$ neV (68% CL) and for the 251 keV resonance was $\omega\gamma = (482 \pm 82)$ μeV . For more details, please see Boeltzig (2016).

4.2.2 $^{23}\text{Na}(p,\alpha)^{20}\text{Ne}$

First studies of the resonances of astrophysical interest in the $^{23}\text{Na} + p$ system were performed by Zyskind et al. (1981) and Görres et al. (1989). The latter was among the first to directly search for a resonance around $E_{\text{lab}} = 144$ keV, which is thought to dominate the $^{23}\text{Na}(p,\alpha)^{20}\text{Ne}$ reaction rate at temperatures relevant for globular cluster nucleosynthesis. However, only tentative upper limits to the resonance strength have been placed by different studies, depending on the value of the unknown proton momentum transfer value I_p . The current recommended rate, obtained assuming $I_p = 2$, is $\omega\gamma \leq 2.8$ neV (Hale et al. (2004)). Indeed, the Boeltzig et al. (2019) measurement of $\omega\gamma$ for the (p, γ) channel suggests values of $I_p = 2$ or 3. Recent work by Marshall et al. (2023) has found a different energy for the excited state involved in the resonant capture, thus shifting the energy of the resonance in the center of mass from $E_{\text{c.m.}} = 138$ keV down to 133 keV. The authors suggest that this could also have an impact on the (p, γ) channel reaction rate. Moreover, the higher lying resonance around 170 keV, which has a contribution only for the (p, α) channel, was slightly moved

from 169.5 to 168.1 keV center-of-mass energy by Marshall et al. (2023). Considering the very low upper limit to the $E_{\text{c.m.}} = 133$ keV resonance strength, the expected rate is too low to be observed from surface laboratories, due to the poor signal-to-background ratio.

In the near future, the ELDAR (burning questions on the origin of the Elements in the Lives and Deaths of sARs) UKRI ERC StG (EP/X019381/1) will study the $^{23}\text{Na}(p,\alpha)^{20}\text{Ne}$ reaction at the LUNA400 kV facility. A newly designed LUNA setup optimized for the underground detection of alpha particles using silicon detectors has been developed. The setup will be commissioned in the near future. The following experimental campaign will aim at reducing the uncertainties on the $^{23}\text{Na}(p,\alpha)^{20}\text{Ne}$ cross section and finally determine the contribution of the $E_{\text{c.m.}} = 133$ keV resonance to the reaction rate by measuring its strength.

5 Anodic oxidation of oxygen targets

Solid oxygen targets can be produced by anodic oxidation of tantalum backings in water. This technique is well-known for producing targets with a precise stoichiometry (Ta_2O_5), and homogeneous thickness. Tantalum disks are cleaned in a bath of 20% citric acid solution in water for 1 h at 90 °C and then mounted in the anodizing apparatus. The anodization setup is described in Caciolli et al. (2012) and a detail is shown in Figure 7. A gold coated basket acts as a cathode by the connection with a Direct Current (DC) power supply. This is controlled by Labview software using a Proportional–Integral–Derivative (PID) controller. The Ta backing acts as the cathode and is grounded. The solution to be anodized is poured onto the backing and the basket is put in contact with the liquid, closing the electric circuit. This generates a current in the water, sputtering oxygen ions onto the Ta backing.

The final target thickness x depends linearly on the applied voltage V according to a phenomenological relationship found by Vermilyea (1953). Due to the thin-film interference, the target changes color as a function of the thickness, allowing an online qualitative thickness estimation. The solution used for target production depends on the reaction to be measured. In Table 1 the main reactions studied with this typology of targets are listed, together with the solution used for the target production.

Doping both ^{17}O and ^{16}O targets with a well known percentage of enriched ^{18}O water allows target monitoring by NRRRA, using a thick-target yield approach. The narrow resonance at $E_p = 151$ keV ($\omega\gamma = (1.0 \pm 0.1)$ meV) was used. Periodic scans at different levels of

TABLE 1 Reaction measured at LUNA with anodized oxygen target with the corresponding solution used in the production.

Reaction	Mother solution used
$^{17}\text{O}(p,\gamma)^{18}\text{F}$	2 mL 90% enriched ^{17}O water + 1 μL 80% ^{18}O water
$^{17}\text{O}(p,\alpha)^{14}\text{N}$	
$^{18}\text{O}(p,\alpha)^{15}\text{N}$	2 mL 99% enriched ^{18}O water
$^{18}\text{O}(p,\gamma)^{19}\text{F}$	
$^{16}\text{O}(p,\gamma)^{17}\text{F}$	2 mL of Ultra Pure natural Water+ 1 μL 80% ^{18}O water

accumulated charge demonstrated that this typology of the target is able to withstand the intense beams provided at LUNA ($I = 200 \mu\text{A}$). Degradation corresponding to a decrease in the target thickness of no more than 20% was observed after irradiation of more than 25 C of accumulated charge. Several proton and alpha capture reactions, listed in Table 1, have been successfully measured at LUNA only thanks to the stability of the oxygen targets under intense irradiation and the low background conditions available at LNGS.

These measured reactions are crucial to exploit the CNO cycle in many different stellar scenarios, and over a wide temperature range (20–1,000 MK), as described in several papers (e.g., (Wiescher et al., 1980; Palmerini et al., 2013 or Clarkson and Herwig, 2020)). One example is the observation of oxygen isotopes in evolved giant stars, which provide important information on the mixing processes taking place in stellar interiors Abia et al. (2017), induced by convection, rotation, and magnetic fields Busso et al. (2010). Oxygen isotopic ratios can also be used to determine the efficiency of these mixing processes and are critical in the classification of stardust oxide and silicate grains that were originally condensed in AGB stars, supernovae, and novae Lugaro et al. (2017). Knowledge of the cross sections and the resonance strengths populated in the temperature range is critical to significantly reduce uncertainties on the reaction rates in the temperature region of interest. The main recent results and the ongoing measurements by the LUNA collaboration are illustrated in the following sections.

5.1 Measurement with ^{17}O oxygen targets

The $^{17}\text{O}(p,\alpha)^{14}\text{N}$ and $^{17}\text{O}(p,\gamma)^{18}\text{F}$ reactions compete in both AGB stars and in novae explosions, and knowledge of their cross sections is key for the determination of the branching ratio between cycle II and III of the CNO cycle in these stellar environments. Depending on the scenario, either the 65 keV or the 183 keV resonance of the ^{18}F compound nucleus dominates the reaction rates. The study of the low energy resonances for both reactions, with the aim to reduce the total uncertainty on reaction rates, has been a key aim of the LUNA collaboration.

An array of nine silicon detectors in close geometry was developed for the measurement of the α -channel, and taking advantage of the charged particles background reduction at LNGS, the strength of the $E_{\text{c.m.}} = 65 \text{ keV}$ resonance was directly measured and found to be $\omega\gamma = (10.0 \pm 1.4 \pm 0.7) \text{ neV}$, almost a factor of two higher than previous estimations done by Sergi et al. (2010) and Sergi et al. (2015) using the Trojan Horse method. Further details on the analysis are reported in Bruno et al. (2016). Using the rate obtained from the new resonance strength, a very good agreement between predictions from intermediate-mass AGB stars and observations in Group-II silicate grains has been obtained. The γ channel was measured using a large-volume HPGe detector in close geometry with the target. The $E_{\text{c.m.}} = 183 \text{ keV}$ resonance strength was measured by Di Leva et al. (2014) with an unprecedented low uncertainty $\omega\gamma = (1.67 \pm 12) \mu\text{eV}$. In addition to this resonance strength, several previously unobserved transitions were observed, aiding in the improvement of nova models. Lower energies that are more significant for AGB scenarios were not able to be studied during this campaign due to the use of a HPGe. In particular, the $^{17}\text{O}(p,\gamma)^{18}\text{F}$ reaction rate at temperatures between 20 and 100 MK,

relevant in the H burning shell of AGB stars, is dominated by a poorly constrained resonance at $E_{\text{c.m.}} = 65 \text{ keV}$. To date, this resonance has only been evaluated by Fox et al. (2005) via indirect methods.

Recently, a new high sensitivity setup, based on a BGO detector with a 3-layer shielding (BPE-Lead-BPE), has been designed that increases the detection efficiency and reduces the intrinsic background with the aim to directly measure this resonance for the first time Piatti, D. and Ciani, G.F. (2023). Further details can be found in Skowronski et al. (2023b). Analysis on the $E_{\text{c.m.}} = 65 \text{ keV}$ is presently ongoing and results will be submitted soon.

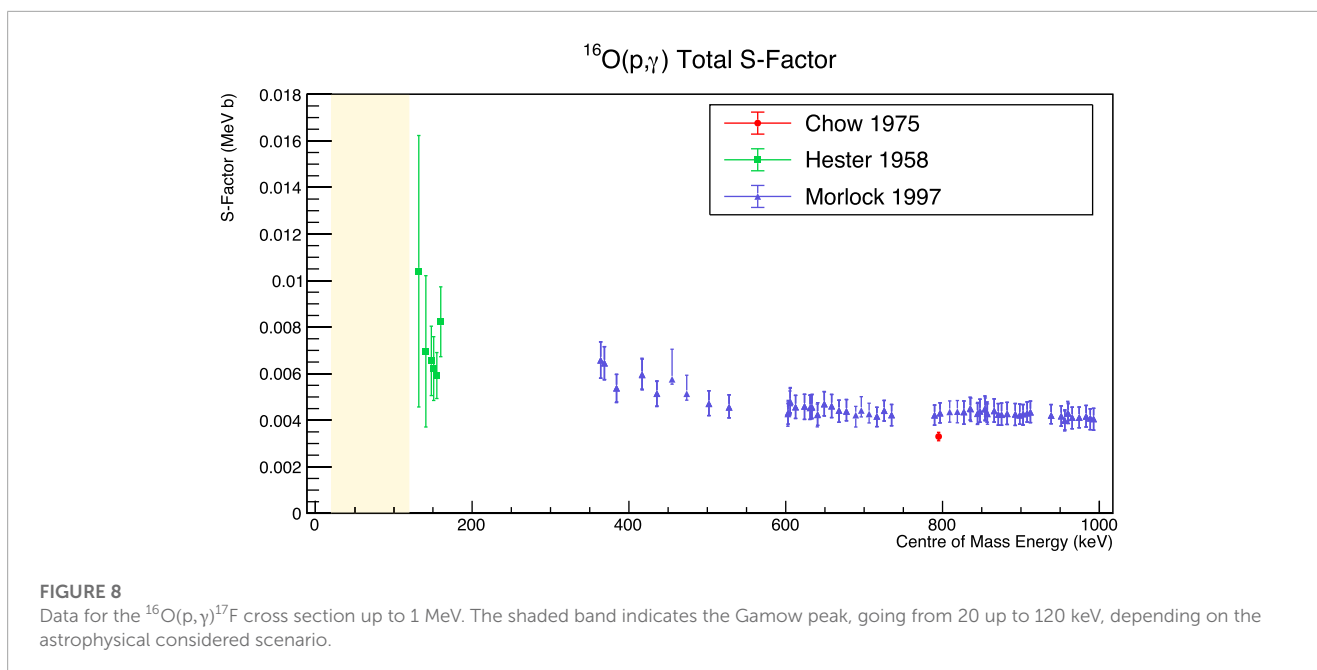
5.2 Measurement with ^{18}O oxygen targets

The $^{18}\text{O}(p,\alpha)^{15}\text{N}$ reaction plays a crucial role in the production of the stable ^{15}N , ^{18}O , ^{19}F isotopes which can be used to trace the mixing and nucleosynthesis processes occurring inside AGB stars and novae. At LUNA, this reaction has been studied in Bruno et al. (2019), using the same setup employed for the $^{17}\text{O}(p,\alpha)^{14}\text{N}$, in the energy range $60 < E_p < 360 \text{ keV}$, the lowest energy for this reaction achieved to date. The $E_{\text{c.m.}} = 90 \text{ keV}$ resonance was found to be a factor of 5 higher than the previously adopted value, and a new, previously unobserved state at $E_{\text{c.m.}} = 106 \text{ keV}$ was required to reproduce the trend of data at low energies. These results significantly reduced the uncertainty in the stellar rate of the $^{18}\text{O}(p,\alpha)^{15}\text{N}$ reaction.

In stellar scenarios, the $^{18}\text{O}(p,\gamma)^{19}\text{F}$ reaction competes with the $^{18}\text{O}(p,\alpha)^{15}\text{N}$ reaction, and an experimental measurement of this reaction was also required in order to determine the ratio of these competing branches. In two separate experimental campaigns, the LUNA collaboration studied the $^{18}\text{O}(p,\gamma)^{19}\text{F}$ reactions across two different energy ranges using two different experimental setups. In Best et al. (2019), the resonance strength of the resonance at $E_{\text{c.m.}} = 90 \text{ keV}$ was measured using a 4π BGO detector, obtaining a value of $(0.53 \pm 0.07) \text{ neV}$. This result was compatible with the previous upper limit in literature, concluding a negligible contribution of this resonance to the stellar reaction rate. In Pantaleo et al. (2021), a higher energy range was studied using the same target with a HPGe detector at 55° , shielded with 15 cm of lead. In this work the resonances at $E_p = 151, 215, 274$ and 334 keV , previously measured only in surface experiments, were investigated, with the observation of numerous, previously unobserved primary transitions. The stellar reaction rate was re-evaluated, including all resonances measured across both campaigns, with no significant difference with respect to previous scenarios since all the new transitions found are too narrow to contribute to the rate.

5.3 Measurement with ^{16}O oxygen targets

The $^{16}\text{O}(p,\gamma)^{17}\text{F}$ reaction plays a fundamental role in the Hot Bottom Burning process of more massive AGB stars. In these stars, the temperature at the base of the convective envelope may reach up to 100 MK and the interplay between H-burning and convective mixing produces important structural changes, the most striking being a substantial increase of the stellar luminosity. At the energies of astrophysical interest, between 20 and 120 keV, the $^{16}\text{O}(p,\gamma)^{17}\text{F}$



reaction ($Q = 600.27$ keV) proceeds through direct capture either to the ground state or to the first excited state, $E_x = 495.33$ keV, of the unstable isotope ^{17}F ($t_{1/2} = 64.49$ s). Angular distributions for the two direct capture gammas have previously been measured in the energy range 0.778–1.840 MeV [Chow et al. \(1975\)](#), [Burtebayev et al. \(2003\)](#), which found that the DC to first excited state transition is strongly anisotropic, and peaks at 90° , while the capture to the ground state is approximately isotropic.

The $^{16}\text{O}(p,\gamma)^{17}\text{F}$ reaction has been the subject of several experimental campaigns by different experimental groups, with several different experimental techniques employed in the measurements. This includes the use of thin transmission solid targets [Chow et al. \(1975\)](#), thick solid targets [Burtebayev et al. \(2003\)](#), gas targets [Morlock et al. \(1997\)](#), experiments in inverse kinematics [Becker et al. \(1982\)](#), and the activation method [Hester et al. \(1958\)](#). Measurements were also made by [Tanner \(1959\)](#) and [Rolf \(1973\)](#). However, there are issues with the stopping power values used by Tanner, and Rolf normalized their results to Tanner's, therefore, these data sets were discarded in the 2021 review of the existing data by [Iliadis et al. \(2021\)](#). The state of the art is shown in [Figure 8](#).

So far, the lowest energy range examined was by [Hester et al. \(1958\)](#), which measured the S(E)-factor in the energy range between 135 and 160 keV, with an average uncertainty of 30%. At higher energies, there is a lack of data between 160 and 360 keV that makes an extrapolation towards the Gamow window difficult. A measurement of the $^{16}\text{O}(p,\gamma)^{17}\text{F}$ reaction by the LUNA group is currently underway to address this lack of data, and aid extrapolations to lower energies. This measurement utilizes ionized oxygen targets made with ultra-pure natural water doped with a well-controlled quantity of ^{18}O enriched water. Two different experimental approaches will be employed: prompt-gamma detection and the activation technique. The prompt-gamma approach will enable the individual measurement of the contributions corresponding to the transitions to the ground state

and the 495.33 keV excited state of ^{17}F , and the measurement of the angular distribution of emitted γ -rays. The activation measurements will provide the total cross section, free from any angular distribution effects or environmental background. Combining the results obtained with the two approaches will reduce the overall systematic uncertainties.

6 Future perspectives with sputtered and implanted targets

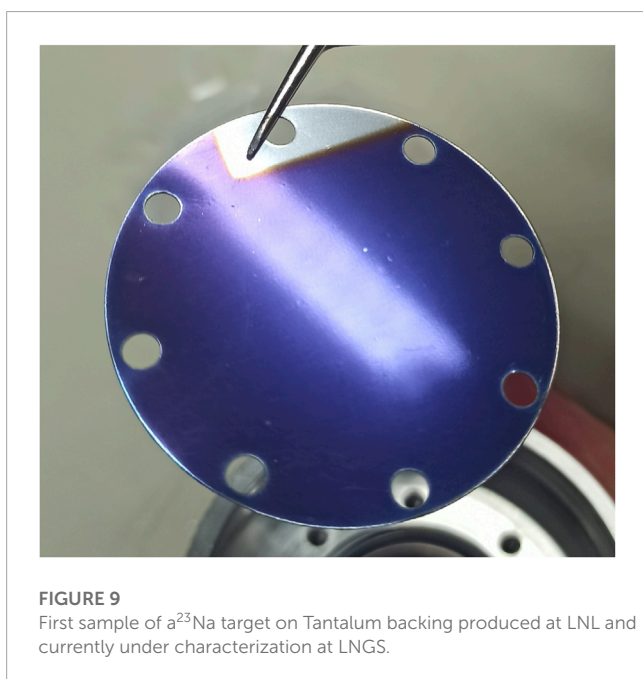
The installation of the 3.5 MV accelerator at the LNGS Bellotti Ion Beam Facility, is an exciting milestone for the LUNA collaboration and offers the ability to address many open questions in nuclear astrophysics. Proton, alpha, and carbon beams will be available, shown in [Table 2](#) adapted from [Sen et al. \(2019\)](#), covering energy ranges not previously accessible at LUNA. The new accelerator and experimental setup are expected to introduce new challenges for solid target measurements. One challenge is the increased power incident on the target, up to 1,000 W compared to the 100 W for the LUNA 400 kV, which is expected to accelerate target degradation. The increased beam energy of LUNA MV may also open new channels of beam induced background, currently not observed at the LUNA 400 kV. To address these challenges, new target typologies are under development in addition to the deep characterization of the purity of the produced targets to better understand any possible background contributions. In parallel, an alternative technique for producing sodium targets is currently under development for future measurement at LUNA 400 kV.

6.1 Nitrogen targets

A new measurement of the $^{14}\text{N}(p,\gamma)^{15}\text{O}$ reaction will be the first activity performed and the new 3.5 MV Singletron[®] of the

TABLE 2 Maximum Beam intensity on target for different beam species at the 3.5 MV Bellotti Ion Beam Facility.

Beam	Intensity (eμA)	
	TV 0.3–0.5 MV.	TV 0.5–3.5 MV
p	500	1,000
⁴ He ⁺	300	500
¹² C ⁺	100	150
¹² C ⁺⁺	60	100

**FIGURE 9**
First sample of a²³Na target on Tantalum backing produced at LNL and currently under characterization at LNGS.

LNGS Bellotti Ion Beam Facility. The $^{14}\text{N}(p,\gamma)^{15}\text{O}$ is the slowest reaction in the CNO cycle and therefore is essential in estimating the lifetime of massive stars as well as determining the CNO neutrino flux from the Sun, which has been recently observed for the first time by the Borexino collaboration (Appel et al., 2022). Despite the efforts of many groups over the years, including pioneering underground measurements made by the LUNA collaboration, e. g., by Formicola et al. (2004), this reaction remains the predominant source of uncertainty when determining solar chemical composition from the direct CNO neutrino flux measurement. The collaboration will measure this reaction at higher energies than the previous study conducted at the LUNA400 kV accelerator. This measurement will present new experimental challenges, primarily from the beam-induced background of several reactions at the higher energies of the LUNA MV. The $^{19}\text{F}(p,\alpha\gamma)^{16}\text{O}$ reaction is anticipated to largest challenge, as fluorine is a common contaminant in tantalum backing, and this reaction has a well-known resonance at $E_p = 340$ keV. This resonance produces a sharp peak at 6.13 MeV, very close to the 6.17 MeV secondary peak of interest in the $^{14}\text{N}(p,\gamma)^{15}\text{O}$ reaction. The $^{15}\text{N}(p,\alpha\gamma)^{12}\text{C}$ reaction is also expected to be a significant source of beam induced background, coming from the 0.5% of isotopic abundance of ^{15}N in natural nitrogen. This produces

a broad peak at 4.4 MeV in the γ -rays spectrum, hampering the sensitivity to the primary γ -rays of the $^{14}\text{N}(p,\gamma)^{15}\text{O}$ reaction.

Solid targets have primarily been produced via the reactive Magnetron sputtering of Nitride coatings, typically TiN, onto Tantalum backings. This method has proved to produce targets with excellent stability against irradiation with high beam powers and a low concentration of impurities. The higher beam energies achievable at the new facility has motivated the development of new targets produced by sputtering Tantalum Nitride (TaN) coatings using isotopically enriched (99.99%) ^{14}N gas. The switch to a higher Z material is required to reduce the neutron background, in order not to perturb the low background environment where the facility is located at the Hall B of LNGS. However, this switch is anticipated to result in the increase of beam induced background from the aforementioned $^{15}\text{N}(p,\alpha\gamma)^{12}\text{C}$ reaction. The Laboratori Nazionali di Legnaro (LNL) are involved in target development and production of isotopically enriched TaN targets using a dedicated apparatus based on close field reactive magnetron sputtering technology.

6.2 Sodium targets

The LUNA collaboration is currently in the process of exploring new production procedures for sodium targets in collaboration with LNL, for the measurement of the $^{23}\text{Na}(p,\alpha)^{20}\text{Ne}$ reaction. One of the major challenges to the production of sodium targets is the hygroscopic behavior of sodium salts, see section 4.2.1 for further details. New procedures for the production of evaporated and sputtered targets on Ta backings using sodium tungstate (Na_2WO_4) and sodium niobate (NaNbO_3) are primarily focused on reducing the sensitivity of targets to humidity and improving stability under beam irradiation. The first samples are currently being analyzed and characterized at the LUNA400 kV facility at LNGS. A technical paper on the performance of these new targets under an intense proton beam will be available within the end of next year. A picture of a sputtered target sample with very promising stability and purity is shown in Figure 9.

7 Conclusion

In this review, we have reported several production techniques for different solid targets that have been used at LUNA, together with the main processes adopted for target characterization and monitoring. Thanks to the huge experience of the LUNA collaboration in handling solid targets, a large number of measurements relevant to a wide range of stellar scenarios significant for stellar evolution have been performed during the 30 years of experiment life.

High purity and enriched evaporated carbon targets have been used for $^{12/13}\text{C}(p,\gamma)^{13/14}\text{N}$ and $^{13}\text{C}(\alpha,n)^{16}\text{O}$ cross section measurements. The accurate techniques used for target monitoring were crucial for pushing the measurements to the lowest energy point ever directly measured achieving the uncertainties required for astrophysical models.

Thanks to the use of ionized oxygen targets, several proton and alpha burning processes on the three stable oxygen isotopes have

been evaluated, providing unprecedented results for what concerns oxygen isotopes ratio in AGB and novae scenario. A long study has been performed on sodium targets during the $^{23}\text{Na}(p,\gamma)^{24}\text{Mg}$ LUNA campaign. The deep knowledge acquired will be combined with new improved techniques to produce more stable sodium targets for the next measurements in the ELDAR project.

Solid targets will continue to play a significant role in future measurements for the LUNA collaboration and the research for further improvements is currently underway to address the challenges presented by the higher power and energy of the new LUNA MV facility.

Author contributions

CA: Writing—original draft, Writing—review and editing. LB: Funding acquisition, Supervision, Writing—original draft, Writing—review and editing. AB: Formal Analysis, Supervision, Writing—original draft, Writing—review and editing. MC: Writing—original draft, Writing—review and editing. FC: Formal Analysis, Writing—original draft, Writing—review and editing. GC: Conceptualization, Data curation, Formal Analysis, Methodology, Project administration, Supervision, Visualization, Writing—original draft, Writing—review and editing. AC: Writing—original draft, Writing—review and editing. RG: Data curation, Writing—original draft, Writing—review and editing. JM: Funding acquisition, Supervision, Writing—original draft, Writing—review and editing. EM: Conceptualization, Formal Analysis, Writing—original draft, Writing—review and editing. DM: Writing—original draft, Writing—review and editing. DRa: Formal Analysis, Writing—original draft, Writing—review and editing. DRo: Data curation, Formal Analysis, Funding acquisition, Writing—original draft, Writing—review and editing. RS: Conceptualization, Funding acquisition, Supervision, Writing—original draft, Writing—review and editing. JS: Data curation, Formal Analysis, Visualization, Writing—original draft, Writing—review and editing.

References

- Abia, C., Hedrosa, R. P., Domínguez, I., and Straniero, O. (2017). The puzzle of the CNO isotope ratios in asymptotic giant branch carbon stars. *A&A* 599, A39. doi:10.1051/0004-6361/201629969
- Aerts, C., Molenberghs, G., Kenward, M. G., and Neiner, C. (2014). The surface nitrogen abundance of a massive star in relation to its oscillations, rotation, and magnetic field. *Astrophys. J.* 781, 88. doi:10.1088/0004-637X/781/2/88
- Alimonti, G., Anghloher, G., Arpesella, C., Balata, M., Bellini, G., Benziger, J., et al. (1998). Ultra-low background measurements in a large volume underground detector. *Astropart. Phys.* 8, 141–157. doi:10.1016/S0927-6505(97)00050-9
- Ananna, C., Barile, F., Boeltzig, A., Bruno, C. G., Cavanna, F., Ciani, G. F., et al. (2021). Underground measurements of nuclear reaction cross-sections relevant to AGB stars. *Universe* 8, 4. doi:10.3390/universe8010004
- Angulo, C., Arnould, M., Rayet, M., Descouvemont, P., Baye, D., Leclercq-Willain, C., et al. (1999). A compilation of charged-particle induced thermonuclear reaction rates. *Nucl. Phys. A* 656, 3–183. doi:10.1016/S0375-9474(99)00030-5
- Appel, S., Bagdasarian, Z., Basilico, D., Bellini, G., Benziger, J., Biondi, R., et al. (2022). Improved measurement of solar neutrinos from the carbon-nitrogen-oxygen cycle by Borexino and its implications for the standard solar model. *Phys. Rev. Lett.* 129, 252701. doi:10.1103/PhysRevLett.129.252701
- Bair, J. K., and Haas, F. X. (1973). Total neutron yield from the reactions $^{13}\text{C}(\alpha, n)^{16}\text{O}$ and $^{17,18}\text{O}(\alpha, n)^{20,21}\text{Ne}$. *Phys. Rev. C* 7, 1356–1364. doi:10.1103/PhysRevC.7.1356
- Balibrea-Correa, J., Ciani, G., Buompane, R., Cavanna, F., Csedreki, L., Depalo, R., et al. (2018). Improved pulse shape discrimination for high pressure ^3He counters. *Nucl. Instr. Meth. Phys. Res. A* 906, 103–109. doi:10.1016/j.nima.2018.07.086
- Becker, H., Kieser, W., Rolfs, C., Trautvetter, H., and Wiescher, M. (1982). Resonance strengths of some light nuclei. *Zeitschrift für Physik A Hadrons Nucl.* 305, 319–323. doi:10.1007/bf01419080
- Best, A., Pantaleo, F., Boeltzig, A., Imbriani, G., Aliotta, M., Balibrea-Correa, J., et al. (2019). Cross section of the reaction $^{18}\text{O}(p,\gamma)^{19}\text{F}$ at astrophysical energies: the 90 keV resonance and the direct capture component. *Phys. Lett. B* 797, 134900. doi:10.1016/j.physletb.2019.134900
- Bisterzo, S., Gallino, R., Käppeler, F., Wiescher, M., Imbriani, G., Straniero, O., et al. (2015). The branchings of the main s-process: their sensitivity to α -induced reactions on ^{13}C and ^{22}Ne and to the uncertainties of the nuclear network. *Mon. Not. R. Astron. Soc.* 449, 506–527. doi:10.1093/mnras/stv271
- Boeltzig, A. (2016). *Direct measurements of the $^{23}\text{Na}(p,\gamma)^{24}\text{Mg}$ cross Section at stellar energies*. Italy: Ph.d., Gran Sasso Science Institute.
- Boeltzig, A., Best, A., Pantaleo, F., Imbriani, G., Junker, M., Aliotta, M., et al. (2019). Direct measurements of low-energy resonance strengths of the $^{23}\text{Na}(p,\gamma)^{24}\text{Mg}$ reaction for astrophysics. *Phys. Lett. B* 795, 122–128. doi:10.1016/j.physletb.2019.05.044
- Brown, T., Deryckx, K., García, A., Sallaska, A., Snover, K., Storm, D., et al. (2009). Properties of ^{23}Na implanted targets. *Nucl. Instr. Meth. Phys. Res. B* 267, 3302–3308. doi:10.1016/j.nimb.2009.06.122

Funding

The author(s) declare financial support was received for the research, authorship, and/or publication of this article. This work was supported by INFN. RS acknowledges funding from STFC (grant ST/P004008/1). LB, JM, and DRo gratefully acknowledge support by the ELDAR (burning questions on the origin of the Elements in the Lives and Deaths of stARs) UKRI ERC StG (EP/X019381/1). DRa, CA, and DM acknowledge funding from the European Research Council (ERC-StG 2019 #852016).

Acknowledgments

For the purpose of open access, the authors have applied a Creative Commons Attribution (CC BY) licence to any Author Accepted Manuscript version arising from this submission.

Conflict of interest

The authors declare that the research was conducted in the absence of any commercial or financial relationships that could be construed as a potential conflict of interest.

Publisher's note

All claims expressed in this article are solely those of the authors and do not necessarily represent those of their affiliated organizations, or those of the publisher, the editors and the reviewers. Any product that may be evaluated in this article, or claim that may be made by its manufacturer, is not guaranteed or endorsed by the publisher.

- Bruno, C., Aliotta, M., Descouvemont, P., Best, A., Davinson, T., Bemmerer, D., et al. (2019). Improved astrophysical rate for the $^{18}\text{O}(p,\alpha)^{15}\text{N}$ reaction by underground measurements. *Phys. Lett. B* 790, 237–242. doi:10.1016/j.physletb.2019.01.017
- Bruno, C. G., Scott, D. A., Aliotta, M., Formicola, A., Best, A., Boeltzig, A., et al. (2016). Improved direct measurement of the 64.5 keV resonance strength in the $^{17}\text{O}(p,\alpha)^{14}\text{N}$ reaction at LUNA. *Phys. Rev. Lett.* 117, 142502. doi:10.1103/PhysRevLett.117.142502
- Burtebayev, N., Kakhramanov, V., Ibraeva, E., Sagindykov, S., and Zazulin, D. (2003). An investigation of characteristics of the reaction $^{16}\text{O}(p,\gamma)^{17}\text{F}$ at astrophysical energies. *Eurasia Nucl. Bull.* 2, 58–63.
- Busso, M., Palmerini, S., Miorio, E., Cristallo, S., Straniero, O., Abia, C., et al. (2010). On the need for deep-mixing in asymptotic giant branch stars of low mass. *Astrophysical J. Lett.* 717, L47–L51. doi:10.1088/2041-8205/717/1/L47
- Busso, M., Wasserburg, G. J., Nollett, K. M., and Calandra, A. (2007). Can extra mixing in RGB and AGB stars be attributed to magnetic mechanisms? *Astrophys. J.* 671, 802–810. doi:10.1086/522616
- Caciolli, A., Scott, D. A., Di Leva, A., Formicola, A., Aliotta, M., Anders, M., et al. (2012). Preparation and characterisation of isotopically enriched Ta_2O_5 targets for nuclear astrophysics studies. *EPJ A* 48, 144. doi:10.1140/epja/i2012-12144-0
- Carretta, E., Bragaglia, A., Gratton, R. G., Recio-Blanco, A., Lucatello, S., D'Orazi, V., et al. (2010). Properties of stellar generations in globular clusters and relations with global parameters. *Astron. Astrophys.* 516, A55. doi:10.1051/0004-6361/200913451
- Cavanna, F., and Prati, P. (2018). Direct measurement of nuclear cross-section of astrophysical interest: results and perspectives. *Int. J. Mod. Phys. A* 33, 1843010. doi:10.1142/S0217751X18430108
- Cesaratto, M. (2011). *Resonant proton Capture on ^{23}Na and elemental Variations in globular cluster stars*. United States: Ph.D., University of North Carolina at Chapel Hill.
- Chow, H. C., Griffiths, G. M., and Hall, T. H. (1975). The $^{16}\text{O}(p,\gamma)^{17}\text{F}$ direct capture cross section with an extrapolation to astrophysical energies. *Can. J. Phys.* 53, 1672–1686. doi:10.1139/p75-213
- Ciani, G. F., Csedreki, L., Balibrea-Correa, J., Best, A., Aliotta, M., Barile, F., et al. (2020). A new approach to monitor ^{13}C -targets degradation *in situ* for $^{13}\text{C}(\alpha, n)^{16}\text{O}$ cross-section measurements at LUNA. *EPJ A* 56, 75. doi:10.1140/epja/s10050-020-00077-0
- Ciani, G. F., Csedreki, L., Rapagnani, D., Aliotta, M., Balibrea-Correa, J., Barile, F., et al. (2021). Direct measurement of the $^{13}\text{C}(\alpha, n)^{16}\text{O}$ cross section into the s-process gamow peak. *Phys. Rev. Lett.* 127, 152701. doi:10.1103/PhysRevLett.127.152701
- Clarkson, O., and Herwig, F. (2020). Convective H–He interactions in massive population III stellar evolution models. *Mon. Notices R. Astronomical Soc.* 500, 2685–2703. doi:10.1093/mnras/staa3328
- Csedreki, L., Ciani, G., Gyürky, G., Vajda, I., Rajta, I., and Kiss, A. (2020). Precise resonance energies measured for energy calibration of particle accelerator using thin silicon–nitride foils. *Nucl. Instr. Meth. Phys. Res. B* 478, 194–200. doi:10.1016/j.nimb.2020.06.040
- Csedreki, L., Ciani, G. F., Balibrea-Correa, J., Best, A., Aliotta, M., Barile, F., et al. (2021). Characterization of the LUNA neutron detector array for the measurement of the $^{13}\text{C}(\alpha, n)^{16}\text{O}$ reaction. *Nucl. Instr. Meth. Phys. Res. A* 994, 165081. doi:10.1016/j.nima.2021.165081
- D'Antona, F., Vesperini, E., D'Ercole, A., Ventura, P., Milone, A. P., Marino, A. F., et al. (2016). A single model for the variety of multiple-population formation(s) in globular clusters: a temporal sequence. *Mon. Not. R. Astron. Soc.* 458, 2122–2139. doi:10.1093/mnras/stw387
- Davids, C. N. (1968). A study of (α, n) reactions on ^9Be and ^{13}C at low energies(n) reactions on ^9Be and ^{13}C at low energies. *Nucl. Phys. A* 110, 619–636. doi:10.1016/0375-9474(68)90377-1
- Denissenkov, P. A., and Weiss, A. (2004). Globular cluster archaeology: hydrogen-burning nucleosynthesis and extra mixing in extinct stars. *Astrophys. J.* 603, 119–126. doi:10.1086/381387
- D'Ercole, A., Vesperini, E., D'Antona, F., McMillan, S. L. W., and Recchi, S. (2008). Formation and dynamical evolution of multiple stellar generations in globular clusters. *Mon. Not. R. Astron. Soc.* 391, 825–843. doi:10.1111/j.1365-2966.2008.13915.x
- Di Leva, A., Scott, D. A., Caciolli, A., Formicola, A., Strieder, F., Aliotta, M., et al. (2014). Underground study of the $^{17}\text{O}(p,\gamma)^{18}\text{F}$ reaction relevant for explosive hydrogen burning. *Phys. Rev. C* 89, 015803. doi:10.1103/PhysRevC.89.015803
- Drotleff, H. W., Denker, A., Knee, H., Soine, M., Wolf, G., Hammer, J. W., et al. (1993). Reaction rates of the s-process neutron sources $^{22}\text{Ne}(\alpha, n)^{25}\text{Mg}$ and $^{13}\text{C}(\alpha, n)^{16}\text{O}$. *Astrophys. J.* 414, 735. doi:10.1086/173119
- Dubovichenko, S. B., Tkachenko, A. S., Kezerashvili, R. Y., Burkova, N. A., and Dzhaizirov-Kakhramanov, A. V. (2022). $^6\text{Li}(p,\gamma)^7\text{Be}$ reaction rate in the light of the new data of the laboratory for underground nuclear astrophysics. *Phys. Rev. C* 105, 065806. doi:10.1103/PhysRevC.105.065806
- Ferraro, F., Ciani, G. F., Boeltzig, A., Cavanna, F., and Zavatarelli, S. (2021). The study of key reactions shaping the post-main sequence evolution of massive stars in underground facilities. *Front. Astron. Space Sci.* 7. doi:10.3389/fspas.2020.617946
- Formicola, A., Imbriani, G., Costantini, H., Angulo, C., Bemmerer, D., Bonetti, R., et al. (2004). Astrophysical s-factor of $^{14}\text{N}(p,\gamma)^{15}\text{O}$. *Phys. Lett. B* 591, 61–68. doi:10.1016/j.physletb.2004.03.092
- Formicola, A., Imbriani, G., Junker, M., Bemmerer, D., Bonetti, R., Brogгинi, C., et al. (2003). The LUNA II accelerator. *Nucl. Instr. Meth. Phys. Res. A* 507, 609–616. doi:10.1016/S0168-9002(03)01435-9
- Fox, C., Iliadis, C., Champagne, A. E., Fitzgerald, R. P., Longland, R., Newton, J., et al. (2005). Thermonuclear reaction rate of $^{17}\text{O}(p,\gamma)^{18}\text{F}$. *Phys. Rev. C* 71, 055801. doi:10.1103/PhysRevC.71.055801
- Gallino, R., Arlandini, C., Busso, M., Lugaro, M., Travaglio, C., Straniero, O., et al. (1998). Evolution and nucleosynthesis in low-mass asymptotic giant branch stars. II. Neutron capture and the s-process. *Astrophys. J.* 497, 388–403. doi:10.1086/305437
- Gao, B., Jiao, T. Y., Li, Y. T., Chen, H., Lin, W. P., An, Z., et al. (2022). Deep underground laboratory measurement of $^{13}\text{C}(\alpha, n)^{16}\text{O}$ in the gamow windows of the s and i processes. *Phys. Rev. Lett.* 129, 132701. doi:10.1103/PhysRevLett.129.132701
- Gnech, A., and Marcucci, L. E. (2019). Theoretical calculation of the p- ^6Li radiative capture reaction. *Nucl. Phys. A* 987, 1–15. doi:10.1016/j.nuclphysa.2019.04.005
- Görres, J., Wiescher, M., and Rolfs, C. (1989). Hydrogen burning of ^{23}Na in the NeNa cycle. *Astrophys. J.* 343, 365. doi:10.1086/167710
- Gratton, R., Bragaglia, A., Carretta, E., D'Orazi, V., Lucatello, S., and Sollima, A. (2019). What is a globular cluster? an observational perspective. *Astron. Astrophys. Rev.* 27, 8. doi:10.1007/s00159-019-0119-3
- Gratton, R. G., Carretta, E., and Bragaglia, A. (2012). Multiple populations in globular clusters. Lessons learned from the Milky Way globular clusters. *Astron. Astrophys. Rev.* 20, 50. doi:10.1007/s00159-012-0050-3
- Greife, U., Arpesella, C., Barnes, C., Bartolucci, F., Bellotti, E., Brogгинi, C., et al. (1994). Laboratory for underground nuclear astrophysics (LUNA). *Nucl. Instr. Meth. Phys. Res. A* 350, 327–337. doi:10.1016/0168-9002(94)91182-7
- Hale, S. E., Champagne, A. E., Iliadis, C., Hansper, V. Y., Powell, D. C., and Blackmon, J. C. (2004). Investigation of the $^{23}\text{Na}(p,\gamma)^{24}\text{Mg}$ and $^{23}\text{Na}(p,\alpha)^{20}\text{Ne}$ reactions via ($^3\text{He}, d$) spectroscopy. *Phys. Rev. C* 70, 045802. doi:10.1103/PhysRevC.70.045802
- Harissopulos, S., Becker, H. W., Hammer, J. W., Lagoyannis, A., Rolfs, C., and Strieder, F. (2005). Cross section of the $^{13}\text{C}(\alpha, n)^{16}\text{O}$ reaction: a background for the measurement of geo-neutrinos. *Phys. Rev. C* 72, 062801. doi:10.1103/PhysRevC.72.062801
- He, J., Chen, S., Rolfs, C., Xu, S., Hu, J., Ma, X., et al. (2013). A drop in the $^6\text{Li}(p,\gamma)^7\text{Be}$ reaction at low energies. *Phys. Lett. B* 725, 287–291. doi:10.1016/j.physletb.2013.07.044
- Heil, M., Detwiler, R., Azuma, R. E., Couture, A., Daly, J., Görres, J., et al. (2008). The $^{13}\text{C}(\alpha, n)^{16}\text{O}$ reaction and its role as a neutron source for the s process. *Phys. Rev. C* 78, 025803. doi:10.1103/PhysRevC.78.025803
- Herwig, F. (2005). Evolution of asymptotic giant branch stars. *Annu. Rev. Astron. Astrophys.* 43, 435–479. doi:10.1146/annurev.astro.43.072103.150600
- Hester, R., Pixley, R., and Lamb, W. (1958). Radiative capture of protons in oxygen at 140 to 170 keV. *Phys. Rev.* 111, 1604–1606. doi:10.1103/physrev.111.1604
- Iliadis, C., Angulo, C., Descouvemont, P., Lugaro, M., and Mohr, P. (2021). New reaction rate for $^{16}\text{O}(p,\gamma)^{17}\text{F}$ and its influence on the oxygen isotopic ratios in massive AGB stars. *Phys. Rev. C* 77, 045802. doi:10.1103/PhysRevC.77.045802
- Imbriani, G., Costantini, H., Formicola, A., Vomiero, A., Angulo, C., Bemmerer, D., et al. (2005). S-factor of $^{14}\text{N}(p,\gamma)^{15}\text{O}$ at astrophysical energies. *EPJ A* 25, 455–466. doi:10.1140/epja/i2005-10138-7
- Junker, M., D'Alessandro, A., Zavatarelli, S., Arpesella, C., Bellotti, E., Brogгинi, C., et al. (1998). Cross section of $^3\text{He}(^3\text{He}, 2p)^4\text{He}$ measured at solar energies. *Phys. Rev. C* 57, 2700–2710. doi:10.1103/PhysRevC.57.2700
- Käppeler, F., Gallino, R., Bisterzo, S., and Aoki, W. (2011). The s process: nuclear physics, stellar models, and observations. *Rev. Mod. Phys.* 83, 157–193. doi:10.1103/RevModPhys.83.157
- Kellogg, S., Vogelaar, R., and Kavanagh, R. (1989). $^{13}\text{C}(\alpha, n)^{16}\text{O}$ and $^{14}\text{C}(p, n)$ astrophysical neutron source and sink. *Bull. Am. Phys. Soc.* 34, 1192.
- Kiss, G. G., La Cognata, M., Yarmukhamedov, R., Tursunmakhmatov, K. I., Wiedenhöver, I., Baby, L. T., et al. (2021). Indirect determination of the astrophysical s factor for the $^6\text{Li}(p,\gamma)^7\text{Be}$ reaction using the asymptotic normalization coefficient method. *Phys. Rev. C* 104, 015807. doi:10.1103/PhysRevC.104.015807
- Krause, M., Charbonnel, C., Decressin, T., Meynet, G., and Prantzos, N. (2013). Superbubble dynamics in globular cluster infancy. II. Consequences for secondary star formation in the context of self-enrichment via fast-rotating massive stars. *Astron. Astrophys.* 552, A121. doi:10.1051/0004-6361/201220694
- Lodders, K. (2003). Solar system abundances and condensation temperatures of the elements. *Astrophys. J.* 591, 1220–1247. doi:10.1086/375492
- Lugaro, M., Karakas, A. I., Bruno, C. G., Aliotta, M., Nittler, L. R., Bemmerer, D., et al. (2017). Origin of meteoritic stardust unveiled by a revised proton-capture rate of ^{17}O . *Nat. Astron.* 1, 0027. doi:10.1038/s41550-016-0027
- Marshall, C., Setoodehnia, K., Cinquegrana, G. C., Kelly, J. H., Portillo Chaves, F., Karakas, A., et al. (2023). New constraints on sodium production in globular clusters from the $^{23}\text{Na}(^3\text{He}, d)^{24}\text{Mg}$ reaction. *Phys. Rev. C* 107, 035806. doi:10.1103/PhysRevC.107.035806

- Masha, E., Barbieri, L., Skowronski, J., Aliotta, M., Ananna, C., Barile, F., et al. (2023). First measurement of the low-energy direct capture in $^{20}\text{Ne}(p,\gamma)^{21}\text{Na}$ and improved energy and strength of the $E_{c.m.} = 368\text{keV}$ resonance. *Phys. Rev. C* 108, L052801. doi:10.1103/PhysRevC.108.L052801
- Morlock, R., Kunz, R., Mayer, A., Jaeger, M., Müller, A., Hammer, J., et al. (1997). Halo properties of the first $1/2^+$ state in ^{17}F from the $^{16}\text{O}(p,\gamma)^{17}\text{F}$ reaction. *Phys. Rev. Lett.* 79, 3837–3840. doi:10.1103/physrevlett.79.3837
- Nastasi, M., Mayer, J. W., and Wang, Y. (2014). *Ion beam analysis: fundamentals and applications*. 1st ed. Florida, United States: CRC Press. doi:10.1201/b17310
- Ohring, M. (1992). “The materials science of thin films,” in *Referex engineering* (United States: Academic Press).
- Palmerini, S., Sergi, M. L., Cognata, M. L., Lamia, L., Pizzone, R. G., and Spitaleri, C. (2013). The RGB and AGB star nucleosynthesis in light of the recent $^{17}\text{O}(p,\alpha)^{14}\text{N}$ and $^{18}\text{O}(p,\alpha)^{15}\text{N}$ reaction-rate determinations. *Astrophysical J.* 764, 128. doi:10.1088/0004-637X/764/2/128
- Pantaleo, F. R., Boeltzig, A., Best, A., Perrino, R., Aliotta, M., Balibrea-Correa, J., et al. (2021). Low-energy resonances in the $^{18}\text{O}(p,\gamma)^{19}\text{F}$ reaction. *Phys. Rev. C* 104, 025802. doi:10.1103/PhysRevC.104.025802
- Piatti, D., Chillery, T., Depalo, R., Aliotta, M., Bemmerer, D., Best, A., et al. (2020). Underground experimental study finds no evidence of low-energy resonance in the $^6\text{Li}(p,\gamma)^7\text{Be}$ reaction. *Phys. Rev. C* 102, 052802. doi:10.1103/PhysRevC.102.052802
- Piatti, D., and Ciani, G. F. (2023). Towards a direct measurement of the $^{17}\text{O}(p,\gamma)^{18}\text{F}$ 65 keV resonance strength at LUNA. *EPJ Web Conf.* 279, 11002. doi:10.1051/epjconf/202327911002
- Piotto, G., Bedin, L. R., Anderson, J., King, I. R., Cassisi, S., Milone, A. P., et al. (2007). A triple main sequence in the globular cluster NGC 2808. *Astrophys. J. Lett.* 661, L53–L56. doi:10.1086/518503
- Prantzos, N. (2012). Production and evolution of Li, Be, and B isotopes in the galaxy. *Astron. Astrophys.* 542, A67. doi:10.1051/0004-6361/201219043
- Renzini, A., D’Antona, F., Cassisi, S., King, I. R., Milone, A. P., Ventura, P., et al. (2015). The hubble Space telescope UV legacy survey of galactic globular clusters - V. Constraints on formation scenarios. *Mon. Not. R. Astron. Soc.* 454, 4197–4207. doi:10.1093/mnras/stv2268
- Rolf, C. (1973). Spectroscopic factors from radiative capture reactions. *Nucl. Phys. A* 217, 29–70. doi:10.1016/0375-9474(73)90622-2
- Rolf, C., and Rodney, W. (1988). “Cauldrons in the cosmos: nuclear astrophysics,” in *Theoretical astrophysics* (Chicago: University of Chicago Press).
- Sekharan, K. K., Divatia, A. S., Mehta, M. K., Kerekatte, S. S., and Nambiar, K. B. (1967). $^{13}\text{C}(\alpha,n)^{16}\text{O}$ reaction cross section between 1.95 and 5.57 mev. *Phys. Rev.* 156, 1187–1190. doi:10.1103/PhysRev.156.1187
- Sen, A., Domínguez-Cañizares, G., Podaru, N., Mous, D., Junker, M., Imbriani, G., et al. (2019). A high intensity, high stability 3.5 MV singletronTM accelerator. *Nucl. Instr. Meth. Phys. Res. B* 450, 390–395. doi:10.1016/j.nimb.2018.09.016
- Sergi, M. L., Spitaleri, C., La Cognata, M., Coc, A., Mukhamedzhanov, A., Burjan, S. V., et al. (2010). New high accuracy measurement of the $^{17}\text{O}(p,\alpha)^{14}\text{N}$ reaction rate at astrophysical temperatures. *Phys. Rev. C* 82, 032801. doi:10.1103/PhysRevC.82.032801
- Sergi, M. L., Spitaleri, C., La Cognata, M., Lamia, L., Pizzone, R. G., Rapisarda, G. G., et al. (2015). Improvement of the high-accuracy $^{17}\text{O}(p,\alpha)^{14}\text{N}$ reaction-rate measurement via the Trojan Horse method for application to ^{17}O nucleosynthesis. *Phys. Rev. C* 91, 065803. doi:10.1103/PhysRevC.91.065803
- Seuthe, S., Becker, H., Krauss, A., Redder, A., Rolf, C., Schröder, U., et al. (1987). Production and properties of implanted targets. *Nucl. Instr. Meth. Phys. Res. A* 260, 33–42. doi:10.1016/0168-9002(87)90385-8
- Skowronski, J., Boeltzig, A., Ciani, G. F., Csedreki, L., Piatti, D., Aliotta, M., et al. (2023a). Proton-capture rates on carbon isotopes and their impact on the astrophysical $^{12}\text{C}/^{13}\text{C}$ ratio. *Phys. Rev. Lett.* 131, 162701. (Article accepted for). doi:10.1103/physrevlett.131.162701
- Skowronski, J., Gesuè, R. M., Boeltzig, A., Ciani, G. F., Piatti, D., Rapagnani, D., et al. (2023b). Advances in radiative capture studies at LUNA with a segmented BGO detector. *J. Phys. G.* 50, 045201. doi:10.1088/1361-6471/acb961
- Straniero, O., Gallino, R., and Cristallo, S. (2006). s process in low-mass asymptotic giant branch stars. *Nucl. Phys. A* 777, 311–339. Special Issue on Nuclear Astrophysics. doi:10.1016/j.nuclphysa.2005.01.011
- Tanabashi, M., Hagiwara, K., Hikasa, K., Nakamura, K., Sumino, Y., Takahashi, F., et al. (2018). Review of particle physics. *Phys. Rev. D* 98, 030001. doi:10.1103/PhysRevD.98.030001
- Tanner, N. (1959). Direct radiative capture of protons by o 16 and ne 20. *Phys. Rev.* 114, 1060–1064. doi:10.1103/physrev.114.1060
- Trippella, O., and Cognata, M. L. (2017). Concurrent application of ANC and THM to assess the $^{13}\text{C}(\alpha,n)^{16}\text{O}$ absolute cross section at astrophysical energies and possible consequences for neutron production in low-mass agb stars. *Astrophysical J.* 837, 41. doi:10.3847/1538-4357/aa5eb5
- Ventura, P., and D’Antona, F. (2006). Does the oxygen-sodium anticorrelation in globular clusters require a lowering of the $^{23}\text{Na}(p,\alpha)^{24}\text{Mg}$ reaction rate? *Astron. Astrophys.* 457, 995–1001. doi:10.1051/0004-6361:20065481
- Ventura, P., D’Antona, F., Criscienzo, M. D., Carini, R., D’Ercole, A., and Vesperini, E. (2012). Super-AGB-AGB evolution and the chemical inventory in ngc 2419. *Astrophys. J. Lett.* 761, L30. doi:10.1088/2041-8205/761/2/L30
- Vermilyea, D. (1953). The kinetics of formation and structure of anodic oxide films on tantalum. *Acta Metall.* 1, 282–294. doi:10.1016/0001-6160(53)90101-1
- Wang, M., Audi, G., Wapstra, A., Kondev, F., MacCormick, M., Xu, X., et al. (2012). The Ame2012 atomic mass evaluation. *Chin. Phys. C* 36, 1603–2014. doi:10.1088/1674-1137/36/12/003
- Wiescher, M., Becker, H., Görres, J., Kettner, K.-U., Trautvetter, H., Kieser, W., et al. (1980). Nuclear and astrophysical aspects of $^{18}\text{O}(p,\gamma)^{19}\text{F}$. *Nucl. Phys. A* 349, 165–216. doi:10.1016/0375-9474(80)90451-0
- Xu, Y., Takahashi, K., Goriely, S., Arnould, M., Ohta, M., and Utsunomiya, H. (2013). Nacre II: an update of the nacre compilation of charged-particle-induced thermonuclear reaction rates for nuclei with mass number $A < 16$. *Nucl. Phys. A* 918, 61–169. doi:10.1016/j.nuclphysa.2013.09.007
- Zeps, V. J., Adelberger, E. G., García, A., Gossett, C. A., Swanson, H. E., Haerberli, W., et al. (1995). Parity mixing of the 0^+-0^- I=1 doublet in ^{14}N . *Phys. Rev. C* 51, 1494–1520. doi:10.1103/PhysRevC.51.1494
- Zyskind, J., Rios, M., and Rolf, C. (1981). The 178 keV resonance in $^{23}\text{Na}(p,\alpha)^{20}\text{Ne}$ and its relevance to the NeNa cycle. *Astrophys. J. Lett.* 243, L53. doi:10.1086/183441